CHEMISTRY OF MATERIALS

Article

pubs.acs.org/cm

Ionic-Diffusion-Driven, Low-Temperature, Solid-State Reactions Observed on Copper Sulfide Nanowires

Matthew T. Mayer,[†] Zachary I. Simpson,[†] Sa Zhou, and Dunwei Wang*

Department of Chemistry, Merkert Chemistry Center, Boston College, 2609 Beacon Street, Chestnut Hill, Massachusetts 02467, United States

Supporting Information

ABSTRACT: Using vertically aligned Cu_2S nanowires as both physical templates and chemical sources, unique heteronanostructures were synthesized by solid-state conversion reactions at low temperatures. At temperatures as low as 105 °C and in the presence of H_2S, segmented nanowires and rod-in-a-tube (RIT) structures were produced. The different morphologies were discovered to depend on the diffusivity of the ions from various metal coatings. In the case where the inward diffusion of outer metal is faster or roughly equivalent to that of Cu^+ outward diffusion, incorporation and subsequent phase segregation occurred to yield segmented nanowires; in instances where Cu^+ diffuses outward more quickly than the metal coating inward, the RIT morphology formed via a Kirkendall-like mechanism. The nanowire−Cu substrate interface was believed to play a unique and crucial role as either a reservoir of additional Cu or as a sink for out-diffusing Cu, depending on the nature of the reaction. Full conversion of Cu_2S nanowires to wurtzite ZnS was also demonstrated, with the complete displacement of Cu back into the Cu substrate. These low-temperature, solid-state conversion reactions show promise as a possible route for synthesizing vertically aligned nanostructures with more complicated compositions.

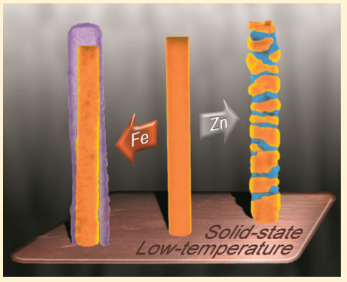

KEYWORDS: *nanowire, nanorods, nanotube, ionic diffusion, solid-state, conversion, copper sulfide, iron, zinc*

INTRODUCTION

When solid-phase reactants are mixed and supplied with sufficient thermal energy, they can react to yield new materials. These diffusion-driven reactions provide a versatile and simple route to products with controllable binary, ternary, or polynary compositions. A large number of semiconducting, superconducting, ionic conducting, and magnetic materials have been prepared using this method.[1] More recently, the structural relationships possible between solid reactants and products have been demonstrated to allow the creation of end materials with targeted morphologies, such as nanowires (NWs) or nanotubes (NTs).[2−5] The nature of solid-state reactions, however, dictates that they proceed at intrinsically slow paces. As such, high temperatures (500−2000 °C), high pressures, or combinations of the two are usually necessary, greatly limiting where and how the method can be employed. For example, works by Gösele et al. demonstrated the Kirkendall effect formation of hollow structures resulting from heating interfaces between metal oxide heterostructures at temperatures in the range of 500−800 °C.[2,6] Others have used similar thermally activated solid-state diffusion processes to form unique nanostructures, including Lieber et al.,[7] Wang et al.,[8] Buhro et al.,[9] and others.[10−12] In each case, temperatures over 500 °C were needed to overcome the significant thermal barrier to diffusion. In the meantime, conversion of nanostructures has been demonstrated using solution-based (wet) chemistry at significantly lower temperatures, solvent- or solute-mediated ion exchange being an important enabling factor.[3,5] For instance, researchers have employed chemical reagents to selectively extract chalcogen anions,[13] or metal cations,[14,15] leaving the nanocrystal size and shape intact in the converted product. Solvent-free all-solid-state reactions of nanomaterials have been comparatively rare.

Herein, using Cu_2S NWs as the model starting material, we report a novel phenomenon that enables solvent-free solid-state reactions under ambient pressure at temperatures as low as 105 °C. Driven by the diffusivity of metal ions in a stable S sublattice, these reactions are shown to yield either unique heteronanostructures such as rod-in-a-tube (RIT) and segmented NWs or fully converted NWs. This mechanism holds promise as new conversion chemistry for the production of nanostructures with desired morphologies and compositions.

Central to the discovery are Cu_2S NWs formed on Cu following a cation-vacancy-diffusion model we recently described.[16] This mechanism is facilitated by the high diffusivity of Cu^+ within Cu_2S that has hindered its utilization in photovoltaics[17−19] but has allowed for its application in memory storage devices[20−23] and solution-phase ion-exchange reactions.[14,15] In the present study, we further exploit the diffusivity and show that this unique property can be used to create nanostructures more complex than simple NWs or nanorods. By utilizing the Cu_2S NWs as a template, we were able to achieve the synthesis of three distinct morphologies (i.e., RITs, segmented NWs, and fully converted NWs) at

Received: August 27, 2011
Revised: October 11, 2011
Published: October 20, 2011

temperatures significantly lower than those normally required for solid-state reactions, which we distinguish from the well-established but fundamentally different solution-based approaches.[14,15] Interestingly, the reactions were found to exhibit a novel dependence on the basal interface between the nanowire and the Cu substrate, across which Cu transport takes place.

EXPERIMENTAL SECTION

Cu_2S Nanowire Synthesis. The synthesis of Cu_2S NW arrays has been described previously.[16] Briefly, Cu foils (99.9%, Alfa Aesar) were anodically polished in orthophosphoric acid (Alfa Aesar, 85% w/w aq.), rinsed well in water, and dried thoroughly in an N_2 stream. They were then placed inside a homemade tube reactor and exposed to a gas mixture of N_2, O_2, and H_2S (Airgas, 99.5% chemically pure) at flow rates of 160, 80, and 12 standard cubic centimeters per minute (sccm), respectively, with the N_2 being bubbled through water to provide humidity. At room temperature and ambient pressure, a continuous Cu_2S film developed across the Cu substrate, from which vertically aligned Cu_2S NWs emerged over the course of several hours. An extended reaction duration of approximately 36 h can yield NW lengths upward of 5 μm.

Metal Deposition. Fe was sputtered onto the as-grown Cu_2S NWs using an AJA International ATC Orion 8 sputtering system. Deposition times ranged from 5 to 25 min, resulting in coating thicknesses of approximately 20 nm. The deposition rate was approximately 0.3 Å/s in all instances of Fe deposition. Zn was thermally evaporated onto as-grown Cu_2S using a Sharon Vacuum evaporation system. The thicknesses of the Zn coatings were varied between 20 and 120 nm.

Synthesis of Cu–Fe–S Rod-in-a-Tube Structures. As-deposited Cu_2S/Fe NW arrays were placed in a tube furnace (Lindberg/Blue M model TF55035A-1), purged with N_2 gas (250 sccm), then heated to 105 °C at a rate of 26 °C/min and held at this point for 30 min in the presence of N_2 (250 sccm) and H_2S (12 sccm; note: H_2S is highly toxic and flammable). After 30 min had elapsed, the lid of the furnace was opened and the chamber was allowed to cool to RT.

Synthesis of Segmented Cu_2S–ZnS and ZnS Nanowires. The annealing procedure for Zn-coated Cu_2S was similar to that of Fe-coated NWs, except that the Zn incorporation was found to take place with or without the presence of H_2S. In this case, the heating rate was approximately 50 °C/min, and the final temperature was varied in the range 105–200 °C. Reaction times were fixed at 30 min.

Structural Characterization. Micrographs, energy-dispersive X-ray spectroscopy measurements, and electron diffraction patterns were obtained using a JEOL 2010F transmission electron microscope with an electron acceleration voltage of 200 kV, equipped with an Oxford Inca EDS spectrometer.

Statistical Studies of the Nanostructure Sizes. For the statistical determination of nanostructure diameter change upon heating, at least 100 measurements were performed by transmission electron microscope (TEM) observation of two different Cu_2S NW specimens, followed by 100 measurements after heat treatments on metal-coated Cu_2S.

RESULTS AND DISCUSSION

Fe–Cu_2S System. As shown in Figure 1, the RIT morphology comprises a rod and a tube, each being a discrete structure, produced through the conversion of an Fe-coated Cu_2S nanowire by heating in an environment of H_2S and N_2 gases. Our interest in the Fe–Cu_2S system was prompted by the potential of pyrite (FeS_2),[24–26] chalcopyrite ($CuFeS_2$),[27] and related materials in electronic, magnetic, and energy-related applications. To the best of our knowledge, NWs belonging to this class of materials, particularly those in a vertically aligned form, have not been reported previously. This deficiency may be corrected using Cu_2S NW arrays as a new synthetic platform.

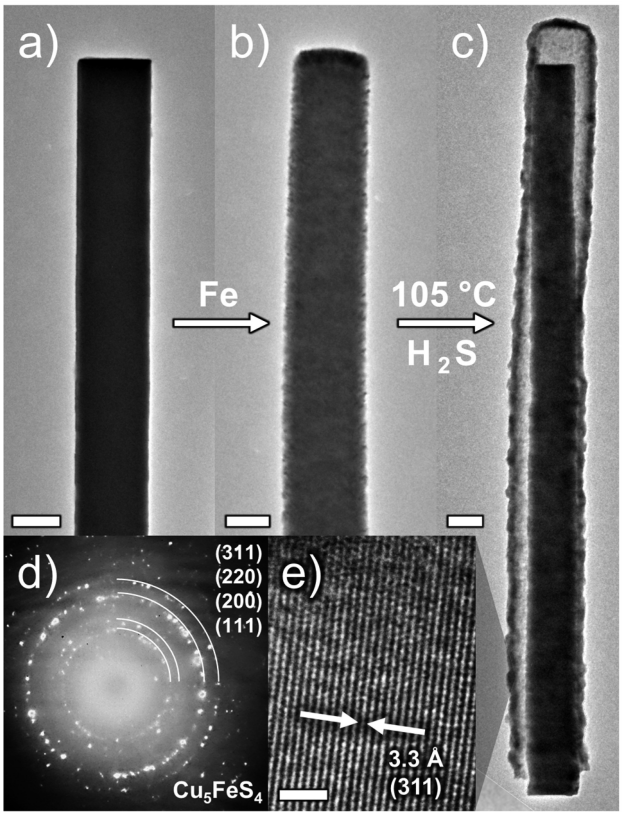

Figure 1. Production of rod-in-a-tube (RIT) morphology from Fe-coated Cu_2S NWs by low-temperature, solid-state reactions depicted by TEM images of (a) as-grown Cu_2S NW, (b) NW after coating by 20 nm sputtered Fe, and (c) the RIT morphology resulting from heating at 105 °C in N_2/H_2S gas for 30 min (scale bars: 100 nm). (d) ED pattern of the tube material, indexed to the Cu_5FeS_4 bornite phase (JCPDS no. 83-2266), with diffraction spots revealing the relatively large grain sizes of the polycrystalline shell. (e) High-resolution TEM shows the crystalline quality of the tube (scale bar: 2 nm).

As a proof-of-concept, we used sputtered thin films of Fe (approximately 20 nm) on preformed Cu_2S NWs as the starting material (Figure 1a and b). A brief (30 min) heating treatment under a gas flow of 5% H_2S and 95% N_2 (by volume) at 105 °C was sufficient to produce the morphology depicted in Figure 1c.

The examination of over 100 structures revealed that the rod and tube in each RIT are clearly separated by a hollow void, distinguishing the RIT morphology from the commonly encountered core/shell morphologies. Low-magnification TEM images showed that the tubes were continuous from the base, where the NWs were physically connected to the Cu substrate from which they grew, to the encapsulated tip (Figure 1c). The tube wall thicknesses varied in the range 25–50 nm. High-resolution TEM indicated that the tubes were polycrystalline in nature, with grain sizes ranging between 5 and 30 nm (Figure 1e, and Figure S1 in the Supporting Information), consistent with the interpretation of the electron diffraction (ED) patterns (Figure 1d). Elemental analysis of the tube material by energy dispersive X-ray spectroscopy (EDS) revealed the average ternary composition of 54.5% Cu, 12.4% Fe, and 33.1% S, in good agreement with the ED characterizations, whose patterns were indexed to the Cu_5FeS_4 phase (JCPDS no. 83-2266). Several factors may contribute to the

dx.doi.org/10.1021/cm202564e | Chem. Mater. 2011, 23, 5045–5051

observed stoichiometry deviation, including the inaccuracies of elemental analysis by EDS and the possibility of excess Cu and Fe within a reasonable range (see Figure S1 of the Supporting Information and its caption for further discussion).

We suggest that the reaction proceeds by a mechanism similar to the Kirkendall effect, in which the highly diffusive Cu^+ ions play a critical role. As shown schematically in Figure 2,

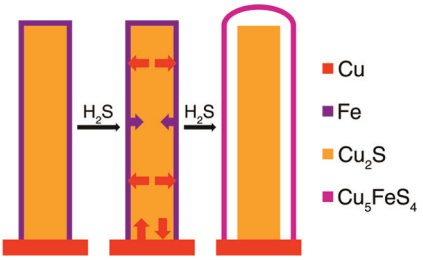

Figure 2. Schematic representation depicting the relative contributions of the diffusive ions to RIT formation. Cu ion diffusion is more pronounced than Fe diffusion, and the S sublattice is stable throughout.

the sulfidation of Fe, in which H_2S serves as an oxidizer, creates ionic vacancies in the shell, driving the outward diffusion of Cu^+. EDS examination revealed the presence of Fe in the encapsulated rods after the reaction was complete, suggesting Fe^{2+} ions also diffuse inward, albeit to a lesser extent. The imbalance between Cu^+ and Fe^{2+} diffusion results in a significant incorporation of Cu^+ by the shell. The accumulation of vacancies at the core–shell interface, as well as the continuous sulfidation of the shell, lead to the separation and expansion which yielded the RIT morphology. The separation likely cuts off the routes of Cu^+ diffusion into the shell and further expansion results from the continued supply of sulfur from the gas phase. In support of these observations, it has been reported that Cu diffuses faster than Fe in chalcopyrite $CuFeS_2$; in the temperature range of 100–300 °C, the upper limits of the diffusion coefficients for Cu and Fe are 9.4×10^{-7} and 5.4×10^{-12} cm^2/s, respectively.[28] Differing from a typical Kirkendall process, however, the core NW is not consumed by the process owing to a continuous supply of Cu from the substrate. This hypothesis is supported by the following observations.

First, when the diffusion of Cu^+ was disrupted, the RIT morphology was less pronounced or entirely absent. We achieved the goal of disrupting Cu^+ diffusion in three ways: electron beam (e-beam) irradiation, the disconnection of Cu_2S NWs from the underlying Cu substrate, and the use of an intermediate blocking layer of Al_2O_3. Our previous studies indicated that Cu^+ ionic behaviors can significantly deviate from their thermodynamically defined behaviors when irradiated by a high-energy e-beam which concentrates Cu^+ within the NWs and hence reduces its mobility.[16] Building on this knowledge, we exposed NWs with Fe coating to TEM e-beam (200 keV in energy) prior to the heating treatment in H_2S and discovered that the RIT morphology did not form. In stark contrast, nearby unexposed NWs on the same substrate reacted normally to yield the RIT morphology (Figure S2a–c of the Supporting Information). We concluded from this set of experiments that the disrupted Cu^+ diffusion by e-beam irradiation is the key reason for the differences. Similarly, when the Cu_2S NWs were separated from the Cu substrate before heating, the RIT morphology in the resulting materials was obviously less pronounced, and the structures showed significant Cu out-diffusion from the exposed end (Figure S3a of the Supporting Information). Because the Cu substrate serves as a reservoir to receive excess Cu^+ ions or to replace Cu^+ deficiencies in the Cu_2S NWs,[16] the disconnection of Cu_2S NWs from the substrate also disrupts Cu^+ diffusion. Finally, we used an interlayer of Al_2O_3, deposited on the NWs before the Fe layer, to disrupt diffusion between the NW and its coating (Figure S4 of the Supporting Information). The resulting shells were found to have a relative concentration of Cu notably lower than that from tubes of typical RITs, coinciding with a significantly less-pronounced expansion and separation from the core NW. We therefore concluded again that Cu^+ diffusion is important to the RIT formation.

Second, statistical studies of the diameters of the starting Cu_2S NWs and the resulting rods and tubes were performed, and it was found that the diameters of the encapsulated rods were approximately the same as those of the NW templates (Figure 3). This observation suggests that there are no

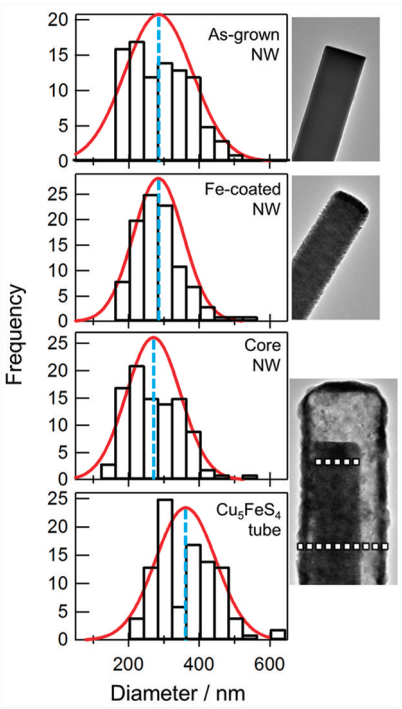

Figure 3. Statistical diameter measurements of the rod-in-a-tube formation process of Fe-coated Cu_2S NWs. Shown are 100 measurements each of as-grown, as-coated, core, and tube morphologies, with a Gaussian fit (red curve) and average (dotted blue line) for each.

measurable changes to the sublattice of Cu_2S NWs during the reaction. Because the inward diffusing Fe is far less than sufficient to replenish the vacancies left by the outward diffusing Cu^+, the only source to draw cations from to maintain the electroneutrality of the system is the underlying Cu support. Lastly, no RITs were observed when Fe-coated Si NWs or ZnO NWs were heated under similar conditions (Figure S5 of the Supporting Information). From this we infer that the sulfidation of Fe alone is insufficient for the RIT formation. Taken as whole, we conclude that a continuous supply of Cu from the substrate is critical to the RIT formation.

dx.doi.org/10.1021/cm202564e | *Chem. Mater.* 2011, 23, 5045–5051

This differentiates the structures from the common zero-dimensional analogues known as "rattle" or "yolk-shell" nanostructures, or nanotubes formed from core/shell nanowires, both of which generally form via a normal Kirkendall process in which the core material is consumed and diminished during the reaction process.[6]

Although the solid-state formation of hollow inorganic structures derived from the reaction of core/shell starting materials by the Kirkendall effect has been previously reported,[6,10,29,30] the temperature at which the RIT forms is highly unusual. This low-temperature reaction is likely enabled by the high diffusivity of Cu^+. The reaction temperature (105 °C) coincides with the Cu_2S phase transition from monoclinic to hexagonal (low- to high-chalcocite), with the latter phase known to exhibit increased Cu mobility.[31−33] Indeed, TEM and ED observations suggest that such a transition may play a role in activating this reaction (Figure S1 of the Supporting Information). We further note that H_2S also plays a critical role in the transformation. Control experiments where the Fe-coated Cu_2S NWs were heated at 105 °C without the presence of H_2S produced no significant morphology or crystal structure changes. While more research is needed to fully understand the role of H_2S, it is believed to serve at least two purposes. First, it reacts with Fe to create ionic vacancies in the Fe-shell to drive Cu^+ outward diffusion. Second, continuous reaction between H_2S and the Cu-incorporated Fe-shell leads to the shell expansion and its subsequent disconnection from the NW template. The decomposition of H_2S likely drives further oxidation of multivalent Fe ions to maintain electroneutrality once the Cu^+ diffusion pathway is broken. Afterward, the shell continues to expand until a thermodynamically stable phase of the Cu−Fe−S system is formed (bornite).

Notwithstanding the fact that ionic exchange reactions at similarly low temperatures in solutions have been reported,[14,15] where the exchange is driven by ionic solubility effects, reports of low-temperature, solid-state, diffusion-driven reactions in solvent-free systems are rare.[34−36] Thus, our results are new and significant. They demonstrate the potential of using Cu_2S NWs as both physical templates and chemical sources to generate high-quality, closed-end, hollow tubes which may be harvested for use in various applications.

Zn−Cu_2S System. To further validate the hypothesis that Cu^+ diffusion enables low-temperature, solid-state reactions, we next examined a system where the inward ion diffusion was comparable to the outward diffusion. For this experiment, we used Cu_2S NWs coated with Zn because Zn^{2+} is of similar size to Cu^+ and has been observed to exhibit appreciable diffusivity within a sulfide sublattice.[37−39] We were also interested in the Zn−Cu_2S system because ion incorporation into Cu_2S could produce new synthetic routes to complex chalcogenides for energy conversion applications, such as Cu_2ZnSnS_4 (CZTS),[40,41] the production of which in a vertically aligned nanowire form remains a challenge.[42] The result was distinctly different from the Fe−Cu_2S system.

As shown in Figure 4, a segmented-NW morphology was obtained when Zn-coated Cu_2S NWs were heated at 105 °C for 30 min in the presence of H_2S. The dark segments in the bright-field TEM images (Figure 4a and b) were identified as Cu_2S, and the gray ones as ZnS, by an EDS line scan across the segments (Figure 4d). The ZnS segments appeared bright and more obvious in the dark-field TEM images (Figure 4c). The ED pattern obtained from a ZnS segment was indexed to the wurtzite phase (Figure 4e, inset). As is evidenced by both the

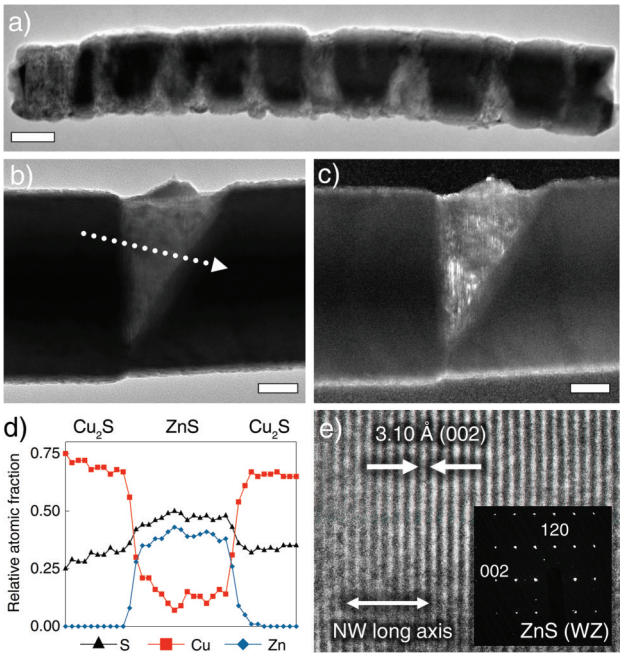

Figure 4. Solid-state reaction of Zn-coated Cu_2S NWs. (a) TEM image showing the overall segmented incorporation of Zn into the NWs (scale bar: 100 nm). Detailed bright-field (b) and dark-field (c) images show the abrupt interfaces between segments and the high degree of crystallinity in the ZnS regions (scale bars: 50 nm). (d) EDS line scan (path shown as dotted arrow in b) showing the Cu_2S and ZnS compositions and abrupt nature of the transition. (e) A high-resolution image of the ZnS region shows lattice-resolved spacing along the NW long axis attributable to the wurtzite phase, as confirmed by the ED pattern (inset).

TEM images and the EDS line scan, the interfaces between the ZnS and Cu_2S segments were abrupt. Interestingly, statistical analysis showed that the average diameters of the ZnS segments were consistent with the original Cu_2S NW diameters, while those of the Cu_2S segments had increased measurably (Figure 5). We understand the reaction mechanism as follows.

The oxidation of the deposited Zn produces Zn^{2+} ions, which are mobile and can diffuse into the sulfide sublattice to occupy the interstices. In a mechanism akin to phase segregation in a multicomponent system, this diffusion process drives Cu^+ out in a given segment to concentrate in the adjacent areas. The concentrated Cu^+ subsequently reacts with H_2S to form new Cu_2S, increasing the diameters of the Cu_2S segments. The proposed mechanism is schematically depicted in Figure 6 and is supported by the following observations.

Similar to the Fe−Cu_2S system, significantly less pronounced or no conversion was observed when the Cu^+ diffusion was disturbed by e-beam irradiation or the removal of the Cu substrate (Figure S2d−f; Figure S3b and c of the Supporting Information). Distinct from the Fe−Cu_2S system, however, the presence of H_2S was found to play a noncritical role in the conversion process, although it did lead to smoother surfaces (Figure S6 of the Supporting Information). This phenomenon can be explained by the ionic diffusions. Because the reaction with H_2S is not a prerequisite for the Zn^{2+} and Cu^+ diffusion, the segregation takes place with or without H_2S. When H_2S is absent, the excess Cu concentrates on the surface of the Cu-rich segments to yield rough morphologies. When H_2S is present, the dynamic reactions between Cu and H_2S result in smooth surfaces and increased diameters of the Cu-rich segments. That

dx.doi.org/10.1021/cm202564e|*Chem. Mater.* 2011, 23, 5045−5051

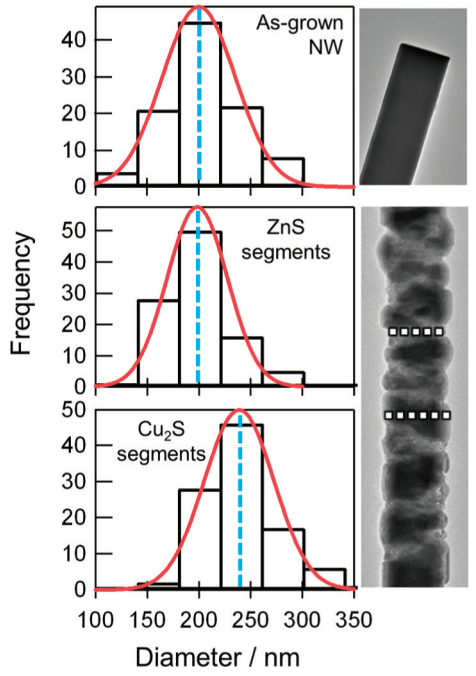

Figure 5. Statistical diameter measurements of the segmented incorporation process for ZnS/Cu_2S heterostructures. Shown are 100 measurements each of as-grown NWs, dark Cu_2S segments, and incorporated ZnS segments, with a Gaussian fit (red curve) and average (dotted blue line) for each.

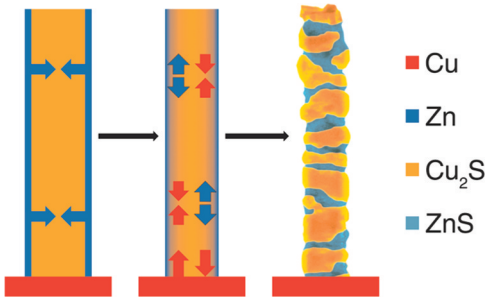

Figure 6. Schematic representation depicting the ionic diffusion which drives the formation of segmented ZnS/Cu_2S heterostructured NWs. Zn inward diffusion prompts Cu diffusion to either the NW surface or back into the Cu substrate.

H_2S is not critical for the reactions with Zn further suggests that Zn can be oxidized by Cu^+. Indeed, the reaction Zn + Cu_2S → Cu + ZnS is exothermic ($\Delta_r H^\circ = -126.5$ kJ/mol).

The arrangements of the segments in the resulting NWs appeared random and followed no particular patterns. In addition, we observed increased Zn incorporation when a thicker Zn film was coated on Cu_2S. As such, the segmented NWs described above reflect a partial conversion resulting from an insufficient supply of Zn. To test this understanding, we increased the thickness of Zn up to 90 nm and found that entire Cu_2S NWs were converted to ZnS. Figure 7 shows bright- and dark-field TEM images where the NW body has a predominantly ZnS composition. While some Cu remains, likely in the form of Cu_2S or Cu in the body or on the surface, the amount is far less than what is sufficient to account for the original Cu content in Cu_2S NW template. The only possible route through which the majority of Cu "disappears" is to diffuse back to the Cu support. Such a hypothesis is highly

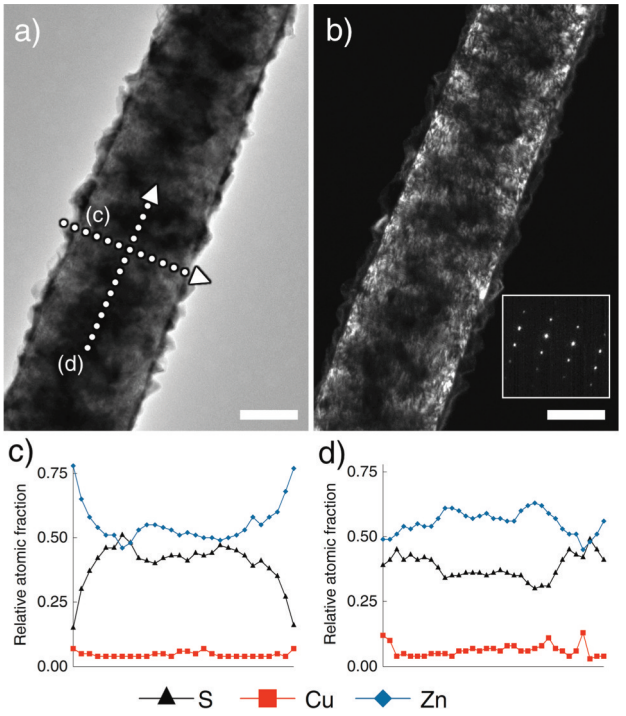

Figure 7. Full conversion from Cu_2S to ZnS NWs. (a) A bright-field TEM image shows the texture of excess Zn on the NW surface, while (b) a dark-field image reveals the intact crystallinity of the NW: (inset) ED pattern that can be indexed to wurtzite ZnS; scale bars: 100 nm. (c) Radial and (d) axial EDS line scans verify the lack of Cu and the presence of ZnS and excess Zn (paths labeled in a).

possible because the attached Cu substrate provides a reservoir for the outward diffusing cations. It is important to emphasize that the diffusive species are ionic in nature. The dark-field image appears to show strain within the NW lattice, presumably due to the lattice mismatch between ZnS and Cu_2S. The amorphous particles on the surface are primarily excess Zn.

The Zn−Cu_2S reaction resulted in morphologies distinct from the RIT structures produced by the Fe−Cu_2S system, demonstrating the versatility of the solid-state process. The resulting segmented NWs suggest a simple reaction process for achieving compositionally modulated NWs which may be shown to demonstrate unique opto- or thermo-electronic properties. In addition, the full conversion from Cu_2S to ZnS NWs may offer a method for achieving, through conversion reactions, NWs of various targeted compositions.

Materials Considerations. In both systems studied here, the solid-state reactions relied on two key characteristics of the Cu_2S NW arrays: (i) appreciable ion diffusion at low temperatures and (ii) an interface between Cu_2S and the Cu substrate across which mass transfer occurs. While Cu_2S is well-known to be an ion-diffusive material, we believe that other chemical systems, even some not typically known to exhibit high ionic diffusivities, could possibly behave similarly in solid-state reactions. In support of this, consider the host of compounds on which solution-based low-temperature exchange reactivity has been demonstrated, which includes a large number of metal chalcogenides and oxides.[3,5,14,15,43,44] Similar to the results of those studies, the nanoscale effect of increased reactivity may allow solid-state reactions of such materials via mechanisms related to what we present here.

dx.doi.org/10.1021/cm202564e | *Chem. Mater.* 2011, 23, 5045–5051

In further comparing the present result to solution-based reaction systems, we acknowledge that those solvent-mediated nanomaterial products often show uniformity and quality better than what we report here, yet we emphasize that fundamental differences between the overall reaction systems differentiate the types of study and likely also contribute to the observed disparity in product quality. For instance, solubility effects of solution-based systems help ensure clean nanoparticle surfaces, whereas our systems relied on physical metal deposition processes which provided relatively imprecise thickness and uniformity control. Additionally, the solution-based studies routinely used nanoparticles on the scale of a few to tens of nanometers, whereas the structures involved in this study possess average diameters in the range of 200−400 nm, and such size considerations will likely affect the reactivity of solids.

CONCLUSIONS

The diffusivity of Cu^+ in the S sublattice renders the Cu_2S system highly unique. The chemistries of the Fe−Cu_2S and Zn−Cu_2S systems provide additional evidence to support our previously proposed cation-vacancy-diffusion model for the Cu_2S NW growth. The existence of ionic diffusion channels between the NWs and the substrate from which the NWs are grown is equally unique. We show here that these channels can be utilized to provide additional Cu^+ (in the case of Fe−Cu_2S reactions) or to store excess Cu^+ (in the case of Zn−Cu_2S reactions). More interestingly, due to their diffusivity differences, distinctly different morphologies (i.e., RIT and segmented NWs) can be obtained. In particular, the RIT morphology is observed for the first time. These structures may prove useful in various applications; the high surface area and inner voids of the RITs may be beneficial in catalysis or sensing applications, and the segmented heterostructures may exhibit useful optoelectronic and thermoelectric properties. More generally, we envision that the high diffusivity of Cu^+ in a S sublattice can be further exploited for a number of important applications, including converting Cu_2S NWs into other compositions (such as CTZS and FeS_2) for solar energy harvesting, or for storing ions with small radii as a means of energy storage. The low temperature at which these solid-state reactions can occur distinguishes this system from others and may be found extremely useful for energy related applications.

ASSOCIATED CONTENT

Supporting Information

Additional representative TEM images of Cu−Fe−S rod-in-a-tube structures, EDS spectra, TEM images from control experiments including e-beam effect, substrate removal, alternative nanowires, and the H_2S gas role. This material is available free of charge via the Internet at http://pubs.acs.org.

AUTHOR INFORMATION

Corresponding Author

*Fax: +1 (617) 552-2705. E-mail: dunwei.wang@bc.edu. Homepage: http://www2.bc.edu/dunwei-wang.

Author Contributions

†These authors contributed equally.

ACKNOWLEDGMENTS

We thank Steve Shepard for technical assistance. This work was supported by Boston College and in part by a research incentive grant.

ABBREVIATIONS

NW, nanowire; NT, nanotube; RIT, rod-in-a-tube; sccm, standard cubic centimeters per minute; TEM, transmission electron microscopy; ED, electron diffraction; EDS, energy dispersive X-ray spectroscopy; CZTS, Cu_2ZnSnS_4

REFERENCES

(1) West, A. R. *Solid State Chemistry and Its Applications*; John Wiley & Sons: New York, 1987.
(2) Fan, H. J.; Knez, M.; Scholz, R.; Nielsch, K.; Pippel, E.; Hesse, D.; Zacharias, M.; Gösele, U. *Nat. Mater.* **2006**, *5*, 627.
(3) Vasquez, Y.; Henkes, A. E.; Chris Bauer, J.; Schaak, R. E. *J. Solid State Chem.* **2008**, *181*, 1509.
(4) Liu, B.; Bando, Y.; Jiang, X.; Li, C.; Fang, X.; Zeng, H.; Terao, T.; Tang, C.; Mitome, M.; Golberg, D. *Nanotechnology* **2010**, *21*, 375601.
(5) Moon, G. D.; Ko, S.; Min, Y.; Zeng, J.; Xia, Y.; Jeong, U. *Nano Today* **2011**, 1.
(6) Fan, H. J.; Gösele, U.; Zacharias, M. *Small* **2007**, *3*, 1660.
(7) Wu, Y.; Xiang, J.; Yang, C.; Lu, W.; Lieber, C. M. *Nature* **2004**, *430*, 61.
(8) Zhou, J.; Liu, J.; Wang, X.; Song, J.; Tummala, R.; Xu, N. S.; Wang, Z. L. *Small* **2007**, *3*, 622.
(9) Trentler, T. J.; Iyer, R. S.; Sastry, S. M. L.; Buhro, W. E. *Chem. Mater.* **2001**, *13*, 3962.
(10) Raidongia, K.; Rao, C. N. R. *J. Phys. Chem. C* **2008**, *112*, 13366.
(11) Fan, H.-M.; Yi, J.-B.; Yang, Y.; Kho, K.-W.; Tan, H.-R.; Shen, Z.-X.; Ding, J.; Sun, X.-W.; Olivo, M. C.; Feng, Y.-P. *ACS Nano* **2009**, *3*, 2798.
(12) Li, Y. J.; Lu, M. Y.; Wang, C. W.; Li, K. M.; Chen, L. J. *Appl. Phys. Lett.* **2006**, *88*, 143102.
(13) Sines, I. T.; Schaak, R. E. *J. Am. Chem. Soc.* **2011**, *133*, 1294.
(14) Luther, J. M.; Zheng, H.; Sadtler, B.; Alivisatos, A. P. *J. Am. Chem. Soc.* **2009**, *131*, 16851.
(15) Sadtler, B.; Demchenko, D. O.; Zheng, H.; Hughes, S. M.; Merkle, M. G.; Dahmen, U.; Wang, L.-W.; Alivisatos, A. P. *J. Am. Chem. Soc.* **2009**, *131*, 5285.
(16) Liu, X.; Mayer, M. T.; Wang, D. *Angew. Chem., Int. Ed.* **2010**, *49*, 3165.
(17) Moitra, K.; Deb, S. *Sol. Cells* **1983**, *9*, 215.
(18) Cassaignon, S.; Pauporté, T.; Guillemoles, J. F.; Vedel, J. *Ionics* **1998**, *4*, 364.
(19) Larson, R. S. *J. Electrochem. Soc.* **2002**, *149*, B40.
(20) Sakamoto, T.; Sunamura, H.; Kawaura, H.; Hasegawa, T.; Nakayama, T.; Aono, M. *Appl. Phys. Lett.* **2003**, *82*, 3032.
(21) Tsuchiya, T.; Oyama, Y.; Miyoshi, S.; Yamaguchi, S. *Appl. Phys. Express* **2009**, *2*, 055002.
(22) Liu, X.; Mayer, M. T.; Wang, D. *Appl. Phys. Lett.* **2010**, *96*, 223103.
(23) Riha, S. C.; Johnson, D. C.; Prieto, A. L. *J. Am. Chem. Soc.* **2011**, *133*, 1383.
(24) Wadia, C.; Wu, Y.; Gul, S.; Volkman, S. K.; Guo, J.; Alivisatos, A. P. *Chem. Mater.* **2009**, *21*, 2568.
(25) Puthussery, J.; Seefeld, S.; Berry, N.; Gibbs, M.; Law, M. *J. Am. Chem. Soc.* **2010**, 716.
(26) Lin, C. W.; Wang, D. Y.; Wang, Y. T.; Chen, C. C.; Yang, Y. J.; Chen, Y. F. *Sol. Energy Mater. Sol. Cells* **2011**, *95*, 1110.
(27) Barkat, L.; Hamdadou, N.; Morsli, M.; Khelil, A.; Bernede, J. *J. Cryst. Growth* **2006**, *297*, 426.
(28) Chen, J. H.; Harvey, W. W. *Metall. Trans. B* **1975**, *6*, 331.
(29) Li, Q.; Penner, R. M. *Nano Lett.* **2005**, *5*, 1720.
(30) Lee, Y.-I.; Goo, Y.-S.; Chang, C.-H.; Lee, K.-J.; Myung, N. V.; Choa, Y.-H. *J. Nanosci. Nanotechnol.* **2011**, *11*, 1455.
(31) Hirahara, E. *J. Phys. Soc. Jpn.* **1951**, *6*, 428.
(32) Evans, H. T. *Am. Mineral.* **1981**, *66*, 807.
(33) Leon, M.; Terao, N.; Rueda, F. *J. Mater. Sci.* **1984**, *19*, 113.
(34) Wang, Q.; Li, J.; Li, G.; Cao, X.; Wang, K.; Chen, J. *J. Cryst. Growth* **2007**, *299*, 386.

(35) Zhang, B.; Jung, Y.; Chung, H.-S.; Van Vugt, L.; Agarwal, R. *Nano Lett.* **2010**, *10*, 149.
(36) Mokari, T.; Aharoni, A.; Popov, I.; Banin, U. *Angew. Chem., Int. Ed.* **2006**, *45*, 8001.
(37) Burton, L. C. *J. Appl. Phys.* **1982**, *53*, 1538.
(38) Cherniak, D. J. *Rev. Mineral. Geochem.* **2010**, *72*, 871.
(39) Sun, H.; Chen, Y.; Wang, X. *J. Nanopart. Res.* **2011**, 97.
(40) Katagiri, H.; Jimbo, K.; Maw, W. S.; Oishi, K.; Yamazaki, M.; Araki, H.; Takeuchi, A. *Thin Solid Films* **2009**, *517*, 2455.
(41) Todorov, T. K.; Reuter, K. B.; Mitzi, D. B. *Adv. Mater.* **2010**, *22*, E156.
(42) Chan, C. P.; Lam, H.; Leung, K. K.; Surya, C. *J. Nonlinear Opt. Phys. Mater.* **2009**, *18*, 599.
(43) Camargo, P. H. C.; Lee, Y. H.; Jeong, U.; Zou, Z.; Xia, Y. *Langmuir* **2007**, *23*, 2985.
(44) Jeong, U.; Camargo, P. H. C.; Lee, Y. H.; Xia, Y. *J. Mater. Chem.* **2006**, *16*, 3893.